Biosensors and Bioelectronics 90 (2017) 251–257

Contents lists available at ScienceDirect

Biosensors and Bioelectronics

journal homepage: www.elsevier.com/locate/bios

DNA tetrahedral scaffolds-based platform for the construction of electrochemiluminescence biosensor

Qiu-Mei Feng, Zhen Zhou, Mei-Xing Li, Wei Zhao*, Jing-Juan Xu*, Hong-Yuan Chen

State Key Laboratory of Analytical Chemistry for Life Science and Collaborative Innovation Center of Chemistry for Life Sciences, School of Chemistry and Chemical Engineering, Nanjing University, Nanjing 210023, PR China

ARTICLE INFO

Keywords:
DNA tetrahedral scaffolds
Electrochemiluminescence
Surface plasmon resonance
CdS quantum dots
Au nanoparticles

ABSTRACT

Proximal metallic nanoparticles (NPs) could quench the electrochemiluminescence (ECL) emission of semiconductor quantum dots (QDs) due to Förster energy transfer (FRET), but at a certain distance, the coupling of light-emission with surface plasmon resonance (SPR) result in enhanced ECL. Thus, the modification strategies and distances control between QDs and metallic NPs are critical for the ECL intensity of QDs. In this strategy, a SPR enhanced ECL sensor based on DNA tetrahedral scaffolds modified platform was reported for the detection of telomerase activity. Due to the rigid three-dimensional structure, DNA tetrahedral scaffolds grafting on the electrode surface could accurately modulate the distance between CdS QDs and luminol labelled gold nanoparticles (L-Au NPs), meanwhile provide an enhanced spatial dimension and accessibility for the assembly of multiple L-Au NPs. The ECL intensities of both CdS QDs (−1.25 V vs. SCE) and luminol (+0.33 V vs. SCE) gradually increased along with the formation of multiple L-Au NPs at the vertex of DNA tetrahedral scaffolds induced by telomerase, bringing in a dual-potential ECL analysis. The proposed method showed high sensitivity for the identification of telomerase and was successfully applied for the differentiation of cancer cells from normal cells. This work suggests that DNA tetrahedral scaffolds could serve as an excellent choice for the construction of SPR-ECL system.

1. Introduction

Electrochemiluminescence (ECL) is a process of the luminescence generated by relaxation of exited state molecules that are produced during an electrochemically initiated reaction (Fahnrich et al., 2001; Richter, 2004). In contrast to traditional optical and electrochemical sensors, ECL sensors show unique advantages, such as high sensitivity, low background signal and no need of any external light source (Liu et al., 2015; Shamsi et al., 2016; Yu et al., 2016). Since the first report on the ECL study of semiconductor quantum dots (QDs) by Bard's group in 2002 (Ding et al., 2002), QDs have attracted widespread application in bioanalytical and analytical chemistry because of their excellent optical performance including quantum size-controlled luminescence, symmetrical emission spectra, broad excitation spectra and excellent light stability (Duan et al., 2009; Liu et al., 2007; Miao, 2008; Wang et al., 2016). However, compared with conventional luminescent reagents like luminol or $Ru(bpy)_3^{2+}$, QDs usually suffer from relatively weaker ECL emissions. Thus, the key challenge for the ECL sensor of QDs still lies in the improvement of the sensing performance of ECL luminophores. Aiming at this issue, many strategies have been introduced in the design of QDs based ECL biosensors for signal amplification, such as ECL resonance energy transfer (ECL-RET), in situ activation of QDs, etc. In 2009, our group reported the surface plasmon resonance (SPR) of Au NPs to enhance the ECL emission of CdS QDs. The excitation of SPR in noble metal NPs could cause strong local electric fields that in turn enhance the luminescence emission of QDs. Through altering the distance, the ECL intensities of CdS QDs could be either quenched or enhanced by proximal Au NPs due to the competition between FRET and field enhancement (Shan et al., 2009). The key technique in SPR-ECL study is the spacing distance control on the electrode surface. DNA was usually used since the distance between noble metal and QDs could be exactly calculated through the number of bases. However, the spacing steric of the double stranded DNAs can't be ignored. As a result, the targets conjugated on the double stranded DNAs were crowed and inhibited the binding activity of the targets, leading to the relative poor detection limit (Chen et al., 2014).

In recent years, DNA tetrahedron has been splendid in biological applications because of the three-dimensional scaffold, structural stability, mechanical rigidity, high precision, well-defined spacing and specific orientation (Bergamini et al., 2014; Li et al., 2011; Lu et al.,

* Corresponding author.
E-mail addresses: weizhao@nju.edu.cn (W. Zhao), xujj@nju.edu.cn (J.-J. Xu).

http://dx.doi.org/10.1016/j.bios.2016.11.060
Received 9 August 2016; Received in revised form 14 November 2016; Accepted 25 November 2016
Available online 27 November 2016
0956-5663/

2012; Pei et al., 2014; Yan et al., 2012). DNA tetrahedron possessed the accurate control of recognition units and easily functioned with different chemical moieties or biomolecules, such as metal nanoparticles (Jia et al., 2014; Yan et al., 2012), DNA probes (Li et al., 2015a, 2015b; Miao et al., 2015), fluorescence molecules (Kim et al., 2013a), and antibodies (Yuan et al., 2014). Meanwhile, due to its three-dimensional scaffold, the designed DNA tetrahedron grafting on the electrode surface could reduce the local overcrowding effect with well-defined spacing and enhance spatial positioning range and accessibility of the probes on the electrode surface over linear or stem-loop probe structures (Pei et al., 2010). For example, Zuo's group estimated that the nanospacing between the DNA linker on the top of DNA tetrahedron (5.78 nm edge length) achieved ~5.0 nm (Chen et al., 2014), bringing into 6 times higher capturing amount of horseradish peroxidase than that on the double stranded DNAs based monolayer. In addition, Fan's group further verified that spire DNA tetrahedron-based sensors possessed stronger electrochemistry and fluorescence sensitivity in detection of prostate-specific antigen (Chen et al., 2014), telomerase activity (Li et al., 2015b) and bioactive molecules (Li et al., 2014) than linear DNA or DNA tetrahedron polymer. Recently, Yin's group designed an ECL biosensor with $Ru(phen)_3^{2+}$ as emitter based on tetrahedron structured DNA for the determination of adenosine triphosphate, bringing into low detection limit and sensitivity (Bu et al., 2013).

Inspired by the high mechanical rigidity and structural stability of DNA tetrahedral scaffolds, in this work, a SPR-based ECL sensor was designed using DNA tetrahedral scaffolds as the connector between QDs and metal NPs. CdS QDs-modified electrodes were prepared by dropping and drying CdS QDs suspension on glassy carbon electrode, then thiol-modified DNA tetrahedral scaffolds attached on CdS QDs via Cd-S bond. The telomerase strand primer (TSP) was inserted into DNA tetrahedral scaffolds to perform the telomerase identification with a SPR-based ECL sensor. In the presence of telomerase, TSP would extend at the vertex of DNA tetrahedral scaffolds. Meanwhile, the three-dimensional rigid structure provided higher accessibility and controllability for the assembly of multiple luminol modified Au NPs (L-Au NPs). Once multiple L-Au NPs was introduced to the extended part of TSP on the surface of electrode, the ECL enhancement of CdS QDs was achieved, at the same time a new ECL signal of luminol appeared. The purpose of using two ECL reporters rather than just QDs is to limit the possible interference such as environmental conditions which may influence the signal output and cause false positive or negative error during trace analysis. Compared with single readout system, ratiometric or dual-signal detections have been proved as more accurate methods in biological and environmental analysis (Wu et al., 2016; Zhang et al., 2013). This proposed DNA tetrahedral scaffolds based dual-potential ECL biosensor affords a sensitive and universal platform in bioanalysis.

2. Materials and methods

2.1. Reagents and apparatus

Refer to the Supporting Information.

2.2. Preparation of L-Au NPs and probe DNA-L-Au NPs

Luminol-gold bifunctional nanoparticles (L-Au NPs) with the diameter of 5 nm were prepared according to the previous work (Zhang et al., 2014b). The synthesized L-Au NPs exhibited the characteristic absorption bond of luminol molecule at 250–400 nm and the feature absorption peak at about 525 nm for Au NPs (Fig. S1A, curve c), suggesting the successful synthesis of L-Au NPs.

For the preparation of probe DNA modified L-Au NPs (abbreviated as probe DNA-L-Au NPs), 49 μL probe DNA (1 μM) and 181 μL bbcDNA (10 μM) was pretreated by 10 mM tris(2-carboxyethyl) phosphine hydrochloride (TCEP) to reduce disulfide bonds, then the mixture solution were added to L-Au NPs solution. The obtained solution was stirred for 12 h in order to assure the fastness of Au-S bond. After that, 0.1 M PBS solution containing 3 M NaCl was added to the colloidal solution stepwise and the mixture was finally brought to 0.3 M NaCl. In order to remove excess DNA, the mixture solution was centrifuged and washed with PBS for three times. The final deposition was resuspended in PBS and stored at 4 °C for further use. The assembled probe DNA-L-Au NPs was characterized with UV–vis spectroscopy. When the L-Au NPs were functioned with probe DNA, the UV–vis spectrum showed the characteristic peak of DNA at 260 nm (Fig. S1A, curve d), suggesting the effective assembly of probe DNA-L-Au NPs. Control sequences labelled Au NPs including S7-L-Au NPs, S8-L-Au NPs, S9-L-Au NPs, S10-L-Au NPs, S11-L-Au NPs and S12-L-Au NPs were also assembled using the above procedure.

2.3. Self-assembly of TTSP scaffolds

In this work, DNA tetrahedron inserted with telomerase strand primer (abbreviated as TTSP) scaffolds were formed by one-pot incubation technique with a simple annealing process (Feng et al., 2016; Yan et al., 2012) and the preparation process of TTSP scaffolds was shown in Scheme 1 A. At the beginning, thiol modified three strands (S2, S3, S4) were treated by 10 mM TCEP to cut S-S bond. Then, equimolar amounts of the four constituent oligonucleotides (S1, S2, S3 and S4, the sequences in the Table S1) were combined in TM buffer (10 mM Tris-HCl, 35 mM $MgCl_2$, pH 8.0). The hybridization mixture was heated at 95 °C for 5 min and then cooled to room temperature over 24 h. High temperature could effectively make chain DNA denatured to an open end and improve the hybridization of DNA to expected structures in the process of temperature reduction. Once assembled, the DNA tetrahedron contained TSP at one edge and three thiol groups at other three vertices. Finally, the obtained TTSP scaffolds were purified by ultrafiltration (30 K molecular weight cutoff) to remove the non-conjugated oligonucleotides. In addition, DNA tetrahedral scaffolds (S2S3S4S5, named as T for short) were assembled using the same procedure.

2.4. Gel electrophoresis

Different DNA structures (S1, S2, S3, S4, S1S2S3, S1S2S4, S1S3S4, S2S3S4 and S1S2S3S4) were all incubated at 95 °C for 5 min and then cooled to room temperature over 24 h. Then, the loading samples (the mixture of 7 μL different DNA structures, 1.5 μL 6×loading buffer, and 1.5 μL of UltraPower TM dye) were injected into a 5% native polyacrylamide gel (prepared by 5×TBE buffer). Before injection into the polyacrylamide hydrogel, the loading samples were placed for 3 min. The electrophoresis analysis was run at 100 V for 1 h. After electrophoresis, the obtained board was observed under UV irradiation and photographed with a Molecular Imager Gel Doc XR.

2.5. Preparation of ECL biosensor

The preparation of ECL biosensor was shown in Scheme 1B. Firstly, a glassy carbon electrode (GCE) was applied as a substrate for immobilizing CdS QDs. The synthesis of CdS QDs referred to the Supporting Information. TEM image of the CdS QDs showed an average diameter of 5 nm (Fig. S2), confirming the successful synthesis of CdS QDs. The GCE was polished in sequential order with 1.0, 0.3 and 0.05 μm of alumina power to obtain a mirror-like clean surface and then thoroughly rinsed with distilled water. Subsequently, 10 μL of CdS QDs solution was drop-cast on the surface of GCE and dried to get CdS QDs film modified GCE at room temperature. The obtained CdS QDs-GCE was immersed in TTSP scaffolds solution and incubated overnight at 4 °C to graft the TTSP bioconjugates on the surface of CdS QDs-GCE (named as TTSP-CdS QDs-GCE). After washing with 0.1 M Tris-HCl

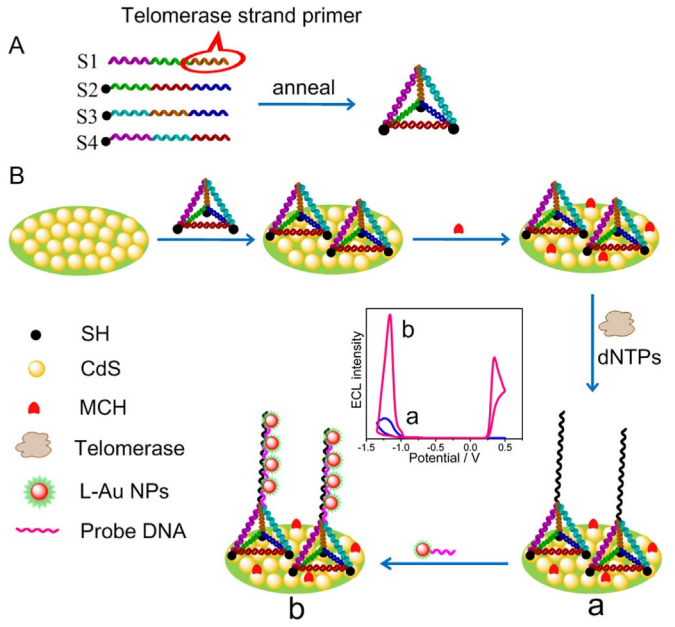

Scheme 1. Schematic illustration of (A) the assembly of TTSP; (B) the ECL sensor configuration strategy.

buffer (pH 7.4), 1 mM 6-mercapto-1-hexanol (MCH) was used for 2 h to block the nonspecific active binding sites of CdS QDs, followed by rinsing with Tris-HCl buffer and stored for the further use.

In the assembly of multiple L-Au NPs, to obtain T-CdS QDs-GCE, the TTSP scaffolds solution was replaced by T scaffolds solution and the other procedures were the same to the above process. The T-CdS QDs-GCE was further incubated with S6 and got S6-T-CdS QDs-GCE.

2.6. Telomerase extracted from HeLa cells

The telomerase extracts from HeLa cells were prepared according to a previously reported work (Zhang et al., 2014a). Firstly, HeLa cells were collected in the exponential phase of growth and washed with PBS. Then, cells were resuspended in 200 μL of ice-cold 3-[(3-cholamidopropyl) dimethylammonio]−1-propanesulfonic acid (CHAPS) lysis buffer (10 mM Tris-HCl, pH 7.5, 1 mM $MgCl_2$, 1 mM ethylene glycol bis(aminoethyl ether)-N,N,N,N tetraacetic acid (EGTA), 0.1 mM phenylmethylsulfonyl fluoride (PMSF), 0.5% CHAPS and 10% glycerol). The mixture was incubated on ice for 30 min and centrifuged for 20 min at 14000 rpm in 4 °C. The supernatant as cell extract was diluted to 200 μL and used immediately for telomerase assay or stored at −80 °C before analysis.

2.7. Analysis procedure

The gained TTSP-CdS QDs-GCE was incubated with telomerase reaction solution containing 5 μL of telomerase extracts and 95 μL of telomerase reaction buffer (20 mM Tris-HCl buffer, pH 8.3, 0.63 mM KCl, 1.5 mM $MgCl_2$, 0.05% Tween 20, 0.1 mM deoxynucleotide solution mixture (dNTPs), 1 mM EGTA) for 2 h. After that, the electrode was incubated with complementary probe DNA-L-Au NPs. Finally, the obtained electrode was rinsed with Tris-HCl buffer and immersed in 0.1 M PBS buffer containing 16 mM H_2O_2 for ECL detection.

3. Results and discussion

3.1. Sensing principle

The SPR-ECL coupling effect of QDs and metallic NPs could be modulated by the distance between them (Shan et al., 2009). Here, DNA tetrahedral scaffolds with rigid nanostructure were applied as rigid linkers to build the SPR-based ECL biosensor. As shown in Scheme 1A, four different single strands DNA (S1-S4) as building blocks were purposefully selected to gain the six edges of the DNA tetrahedron. TSP sequence was implanted in S1 strand and thiol groups were bound at 5′ end of S2, S3 and S4. The principle of this SPR-based ECL biosensor for telomerase assay is illustrated in Scheme 1B. DNA tetrahedral scaffolds containing TSP at one edge and three thiol groups at the other three vertices were grafted on the surface of CdS QDs-GCE via Cd-S bond in highly ordered arrangement. In the presence of telomerase, TSP could be repetitively extended and the obtained pendant linear sequence enabled the hybridization with multiple probe DNA-L-Au NPs. Through monitoring the changing of ECL emission of CdS QDs at −1.25 V (vs SCE), the ECL enhancing efficiency from Au NPs to CdS QDs could be calculated. Meanwhile, a new ECL signal of luminol at +0.33 V (vs SCE) confirmed the successful assembly of L-Au NPs. Due to their upright consistent orientation and rigidity pyramidal structure, DNA tetrahedral scaffolds contributed to a stable and precise regulation of the separation distance between CdS QDs and L-Au NPs. Thus, sensor based on DNA tetrahedral scaffolds possessed a better ECL sensing performance than that of linear DNA. Moreover, the highly arranged TTSP on the surface of electrode made the capturing of probe DNA-L-Au NPs more easily because of the low steric hindrance.

3.2. Characterization of TTSP nanostructure

To confirm the correct formation of TTSP nanostructure after annealing, transmission electron microscopy (TEM), gel electrophoresis, atomic force microscopy (AFM) and dynamic light scattering (DLS) were performed. The TEM images (Fig. 1A and B) show uniform nanostructures with diameter of 10 ± 2 nm, which was close to the calculated TTSP structure (9.86 nm in length, 11.3 nm in diameter). The gel electrophoresis was further applied to verify the formation of TTSP nanostructure in Fig. 1C. TTSP nanostructure (lane a) shifted slower than the combinations of three strands (lanes b-e) and the single strand DNA (lanes f-i). Compared with linear or more compact structures, the increased mass and spatial complexity of the TTSP nanostructure hindered the movements through the pores of the polyacrylamide hydrogel (Yuan et al., 2014). Besides, the TTSP nanostructure was also characterized by AFM and the obtained image showed the tetrahedron in the dried state to be about 4 nm in height (Fig. 1D). Based on 0.34 nm for one base pair (Chen et al., 2014), tetrahedron scaffold with 9.86 nm edge length should be about 8.05 nm in height. However, because of the structure distortion of three-dimensional DNA tetrahedron by the AFM tip and the strong electrostatic interactions with the substrate and dehydration, three-dimensional DNA tetrahedron would collapse to form two-layered DNA structure (Ke et al., 2009). In addition, the four strands nanostructures show perfect uniformity with hydrodynamic size of 12.6 ± 0.7 nm (Fig. 1E), which limited the possibilities of the formation of random DNA structures or impurities. The results were consistent with DNA tetrahedron reported by Ahn and co-workers. (Kim et al., 2013b).

3.3. Characterization of the SPR-based ECL sensor

Fig. 2 displays the ECL responses of different modified electrodes after each step. When the bare GCE was modified with CdS QDs, a distinguished and stable ECL signal appeared at −1.25 V (curve a). Subsequently, with the grafting of TTSP, the ECL signal decreased (curve b), ascribing to the formation of layer with lower conductivity on the surface of electrode. After the incubation of telomerase, the ECL intensity further decreased due to the generation of telomerase-triggered stem elongation product (curve c). While, after the hybridization of probe DNA-L-Au NPs with TSP extension, the ECL signal from

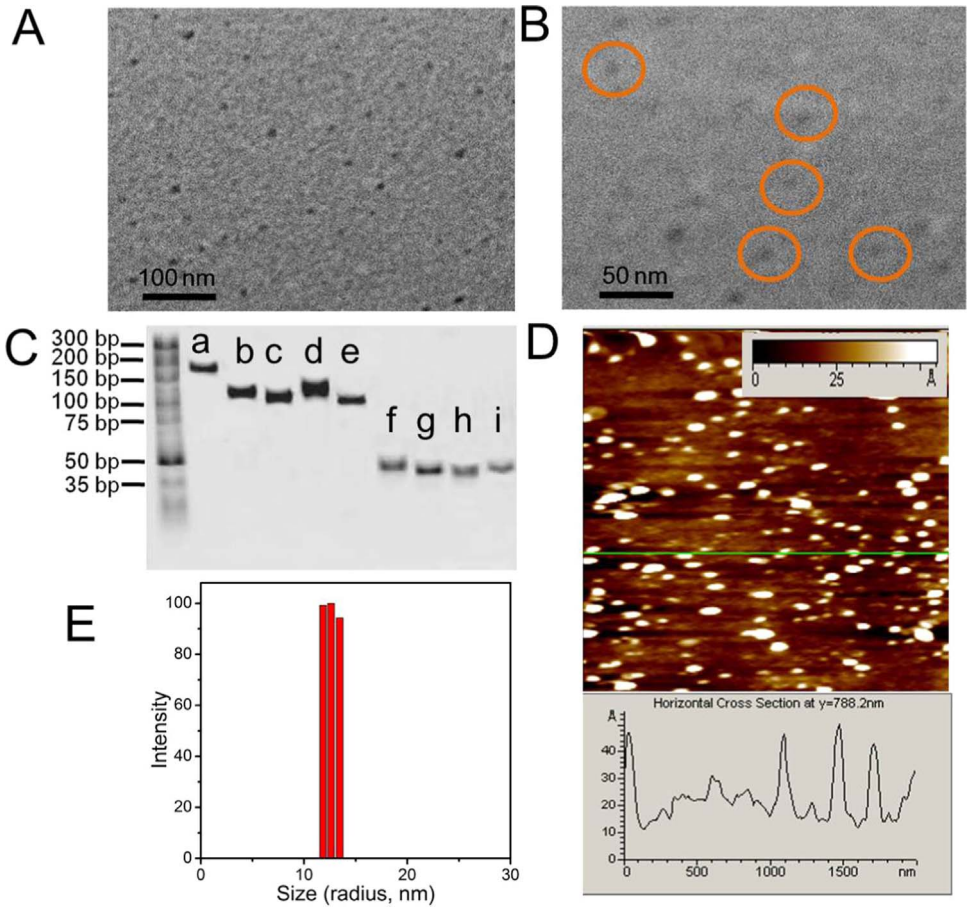

Fig. 1. TEM images of (A) the TTSP and (B) a magnified version. Individual TTSP is circled. (C) Gel electrophoresis image of (lane a) S1S2S3S4 (TTSP), (lane b) S1S2S3, (lane c) S1S2S4, (lane d) S1S3S4, (lane e) S2S3S4, (lane f) S1, (lane g) S2, (lane h) S3, (lane i) S4. (D) AFM image of TTSP. (E) DLS data of the TTSP..

CdS QDs was distinctly enhanced and meanwhile an apparent oxidative-reductive ECL signal from luminol at +0.33 V was brought (curve d), confirming the successful assembly of probe DNA-L-Au NPs and effective interactions of the excited CdS QDs with SPR in Au NPs. In addition, the electrochemical impedance spectroscopy (EIS) characterization of SPR-based ECL sensor was also performed in Fig. S3.

3.4. Comparison of different sensing strategies

According to Li's work, TTSP nanostructure improved the consistently favorable orientation of TSP at the electrode surface, which avoided possible complex entanglement from linear ssTSP (Li et al., 2014). Here in this work, the sensing performance of TTSP based sensor was compared with that of single-strand telomerase strand primer (ssTSP) based sensor for the evaluation of this fabrication strategy. As shown in Fig. 3, under the same conditions, compared with ssTSP based sensor, TTSP based sensor possessed obviously stronger ECL signals. Because of the flexibility of linear ssTSP, it may lie flat on the electrode surface leading to the increase of steric hindrance, electrostatic interaction and low hybridization efficiency (Li et al., 2014; Pei et al., 2010). The hybridization efficiency of ssTSP sensor for probe DNA-L-Au NPs was limited and the corresponding ECL intensity decreased. On the contrary, each TTSP nanostructure could be grafted on the surface of CdS QDs-GCE with upright consistent orientation. Therefore, TTSP nanostructure based sensor could specifically capture much more probe DNA-L-Au NPs and show enhanced ECL signal.

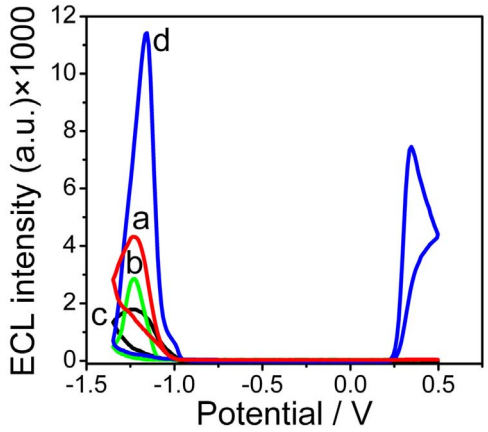

Fig. 2. ECL-potential curves of stepwise modified electrodes: (a) CdS QDs-GCE, (b) TTSP grafting on the CdS QDs-GCE, (c) incubated with telomerase extracts from HeLa cells and (d) hybridization with probe DNA-L-Au NPs.

3.5. Optimization of telomerase elongation time

The telomerase elongation time was evaluated for further detection. In Fig. 4A, both ECL intensities of CdS QDs (curve a) and luminol (curve b) gradually increased with the telomerase elongation time elapsing and reached the platform stage after 80 min. The length of extended primers can be accurately regulated with the incubation time of telomerase. Thus, the hybridization numbers of L-Au NPs could be precisely controlled. To investigate the exact numbers of L-Au NPs

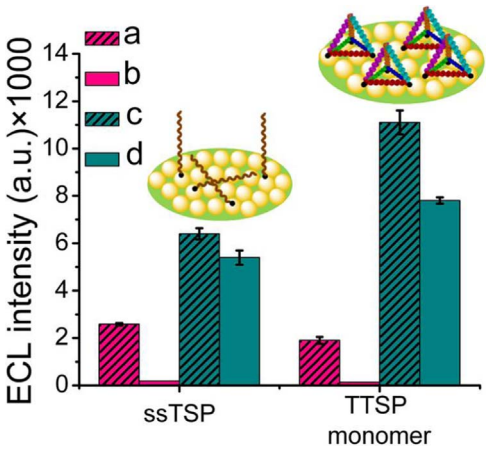

Fig. 3. (A) Bar graph of the ECL intensity for two different sensors: ssTSP and TTSP with telomerase extracted from 20000 HeLa cells. (a) ECL intensity of CdS QDs after the treatment of blank lysis buffer; (b) ECL intensity of luminol after the treatment of blank lysis buffer; (c) ECL intensity of CdS QDs after the treatment of telomerase from HeLa cells; (d) ECL intensity of luminol after the treatment of telomerase from HeLa cells. Inset: schematic illustration of the possible arrangement for ssTSP and TTSP on the surface of CdS QDs-GCE.

modified on the substrate, probe DNA tagged with L-Au NPs (S7-L-Au NPs, S8-L-Au NPs, S9-L-Au NPs, S10-L-Au NPs, S11-L-Au NPs, S12-L-Au NPs) were assembled on S6-T-CdS QDs-GCE to form $(\text{L-Au NPs})_n$ for the fabrication of SPR-based ECL sensor. The ECL intensity of CdS QDs gradually increased with the increase of L-Au NPs number and reached the maximum at n=4 (Fig. 4B). It was known that the emission of CdS QDs was sensitively enhanced by the excitation of SPR in Au NPs in a certain distance. The ECL enhancement efficiency of CdS QDs was diminished along with the increasing number of L-Au NPs because of the distance enlargement between L-Au NPs and CdS QDs. With further increasing of L-Au NPs number 5–6), the ECL emissions of CdS QDs slightly decreased. Because of the unstable of overlong linear DNA, the distance between L-Au NPs and electrode surface may be shortened, and thus the emission of CdS QDs was quenched by proximal Au NPs through FRET. Meanwhile, the ECL intensity of luminol kept enhancing with the increase of L-Au NPs number from 1 to 6, suggesting the shortening of the distance between L-Au NPs and electrode surface won't limit the ECL intensity of luminol. Finally, with 80 min telomerase elongation, 3 or 4 L-Au NPs might assemble on the DNA tetrahedral scaffolds, which resulted in the best ECL response of CdS QDs.

3.6. Analytical performance

On the basis of optimal experimental conditions, telomerase activity from various concentrations of HeLa cells were assayed on the proposed SPR-based ECL sensor using CdS QDs and luminol both as emitters. In Fig. 5A, ECL intensities of both CdS and luminol increased as the HeLa cell concentration increased from 0 to 32000 cells/mL. Both the increment of ECL (△ECL) intensities of CdS QDs and luminol were enhanced along with the increasing of telomerase activity (Fig. 5B). The detection limit of telomerase activity reached 2.03×10^{-9} IU for CdS QDs and 1.45×10^{-9} IU for luminol based on the signal to noise ratio of 3, which was two orders lower than using ELISA kit. The above results indicated that DNA tetrahedral scaffolds-based platform for ECL detection possessed better sensitivity. Meanwhile, the ECL stability of the proposed sensor was also evaluated by monitoring its ECL response toward 5.80×10^{-7} IU telomerase activity extracted from 20000 cells/mL HeLa cells under consecutive cyclic potential scans for fifteen cycles and the result is presented in Fig. S4. It was found that the ECL responses did not appear obvious changes. The ratio relationship of two signal increments ($\triangle ECL_{Luminol}/\triangle ECL_{CdS\ QDs}$) was studied in Fig. S5. The ratio maintained a constant of ca. 0.78 when the telomerase activities were from 2.32×10^{-8} IU to 9.28×10^{-7} IU. The dual-signal system may reduce the false-positive signal and possible interference.

Epigallocatechin-3-gallate (EGCG), which has been reported to induce the apoptosis of cancer cell lines, could effectively reduce the telomerase activity in cancer cells (Punathil et al., 2008; Qian et al., 2013). Fig. 5C shows that the ECL intensities of CdS QDs and luminol were reduced with the concentrations of EGCG from 0 to 200 mg/L, indicating that the intracellular telomerase activity was effectively inhibited by EGCG. In addition, the feasibility of SPR-based ECL sensor for the detection of telomerase activity was further verified using various types of cells, such as A549 (lung cancer), MCF-7 (breast cancer), HL-60 (promyelocytic leukemia), BGC-823 (gastric cancer), QSG-7701 (normal liver) and heated HeLa cells. As shown in Fig. 5D, stronger ECL signals were observed for cancer cells, indicating that cancer cells possessed higher telomerase activities than normal cells (absence of telomerase) and heated HeLa cells (inactivated telomerase). Meanwhile, the telomerase activity from cell extracts was measured via in vitro enzyme-linked immunosorbent assay (ELISA) kit using a standard curve (Fig. S6). The corresponding activity of telomerase extracts in a single cell was estimated to be $2.7\times10^{-11}\pm1.3\times10^{-12}$ IU (A549 cell), $2.4\times10^{-11}\pm1.3\times10^{-12}$ IU (MCF-7 cell), $2.6\times10^{-11}\pm1.3\times10^{-12}$ IU (HL-60 cell), $2.1\times10^{-11}\pm1.3\times10^{-12}$ IU (BGC-823), $2.9\times10^{-11}\pm1.3\times10^{-12}$ IU (HeLa cell) and $9.1\times10^{-13}\pm1.3\times10^{-12}$ IU (QSG-7701 cell). Our designed sensor could be used for the detection of telomerase activity from different cancer cells.

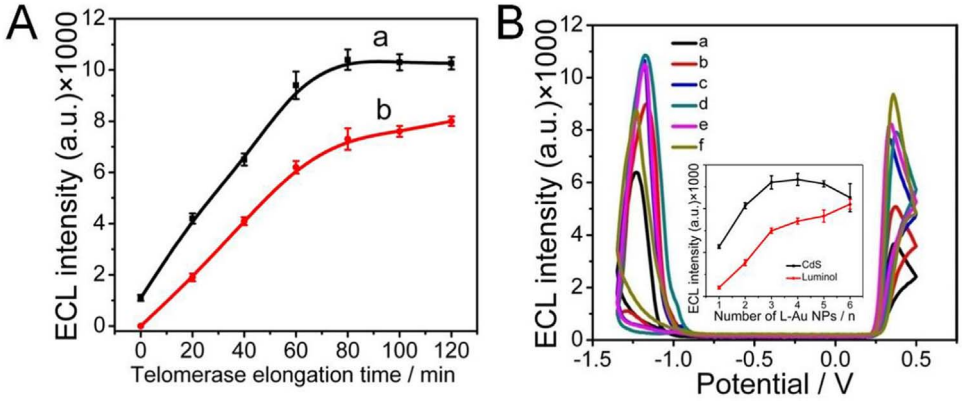

Fig. 4. (A) Relationship between the ECL intensity of (a) CdS QDs or (b) luminol and the telomerase elongation time for TTSP modified CdS QDs-GCE. Telomerase extracts from 20000 Hela cells was analyzed after different telomerase elongation times. (B) ECL-potential curves of the sensing interface with different L-Au NPs numbers (n=1–6). Inset is the corresponding linear curves relationship.

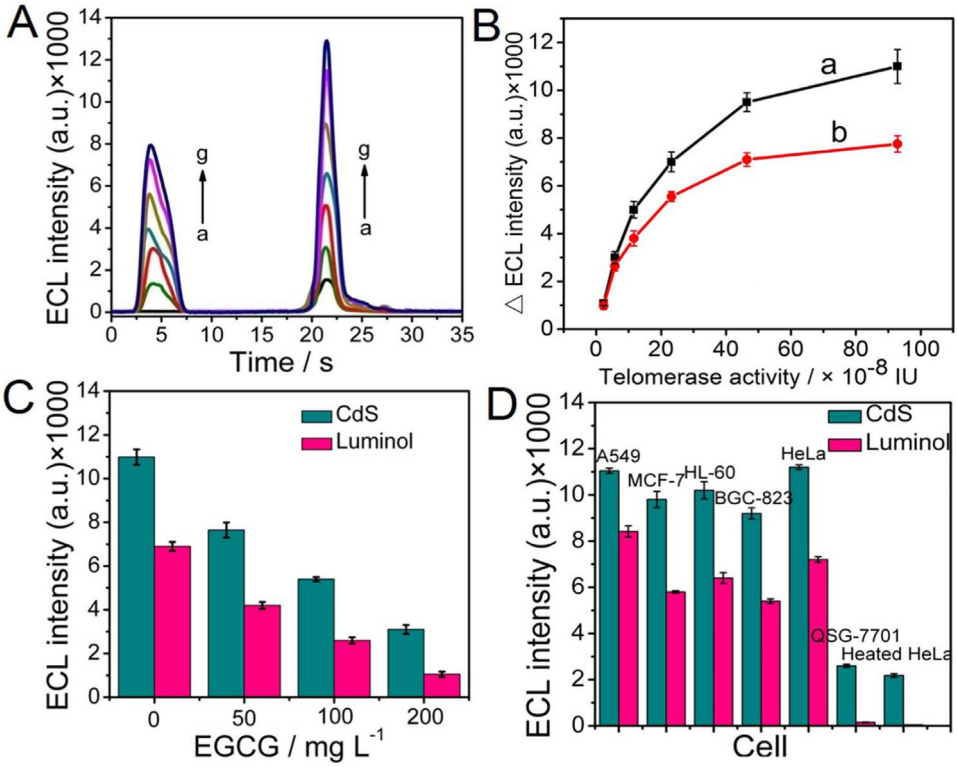

Fig. 5. (A) ECL intensity-time curves at the SPR-based ECL sensor with telomerase extracted from different concentrations of HeLa cells (from a to g: 0–32000 cells/mL). (B) Relationship between △ECL intensity of CdS QDs (a) or luminol (b) and the telomerase activity. ECL measurements were carried out in 0.1 M PBS buffer (pH 7.4) containing 16 mM H_2O_2. Voltage of the photomultiplier tube: −800 V. Scan rate: 100 mV/s. Scan direction: 0 V → 0.5 V → −1.35 V → 0 V. (C) Bar graph of the ECL intensity at the dual-potential ECL sensing interface with telomerase from 0, 50, 100 and 200 mg/L EGCG-treated HeLa cells (20000 cells/mL). (D) Bar graph of the ECL intensity at the ECL sensing interface with telomerase from different kinds of 20000 cells/mL cells lines (from left to right, A549 cells, MCF-7 cells, HL-60 cells, BGC-823 cells, HeLa cells, normal QSG-7701 cells and heated inactivated HeLa cells as a negative control).

4. Conclusions

In this work, we provided a novel SPR-based ECL sensor with DNA tetrahedral scaffolds as platform and multiple L-Au NPs as enhancer for the sensitive differentiation of cancer cells via telomerase activity. The obvious ECL signals enhancement of CdS QDs was attributed to two main reasons. Firstly, DNA tetrahedral scaffolds modified with three thiol groups were anchored on the surface of CdS QDs-GCE, bringing about well-defined spacing and highly ordered arrangement of telomerase extension on the surface of electrode. The rigidity pyramidal structure of DNA tetrahedron also caused the precisely regulation of distance separation between Au NPs and QDs. Secondly, multiple L-Au NPs assembled on DNA tetrahedral scaffolds caused an enhanced SPR-ECL coupling effect which greatly promoted the performance of the sensor. Thus, we believe that DNA tetrahedral scaffolds based ECL sensor opens a promising path in the future study of metal-enhanced QDs luminophores.

Acknowledgments

We gratefully acknowledge the financial support by Ministry of Science and Technology of China (No. 2016YFA0201202), the financial support by the National Natural Science Foundation (NSFC 21327902, 21535003, 21475058).

Appendix A. Supporting information

Supplementary data associated with this article can be found in the online version at doi:10.1016/j.bios.2016.11.060.

References

Bergamini, C., Angelini, P., Rhoden, K.J., Porcelli, A.M., Fato, R., Zuccheri, G., 2014. Methods 67, 185–192.
Bu, N.N., Gao, A., He, X.W., Yin, X.B., 2013. Biosens. Bioelectron. 43, 200–204.
Chen, X.Q., Zhou, G.B., Song, P., Wang, J.J., Gao, J.M., Lu, J.X., Fan, C.H., Zuo, X.L., 2014. Anal. Chem. 86, 7337–7342.
Ding, Z.F., Quinn, B.M., Haram, S.K., Pell, L.E., Korgel, B.A., Bard, A.J., 2002. Science 296, 1293–1297.
Duan, J.L., Song, L.X., Zhan, J.H., 2009. Nano Res. 2, 61–68.
Fahnrich, K.A., Pravda, M., Guilbault, G.G., 2001. Talanta 54, 531–559.
Feng, Q.M., Zhu, M.J., Zhang, T.T., Xu, J.J., Chen, H.Y., 2016. Analyst 141, 2474–2480.
Jia, Y.M., Wei, B.M., Duan, R.X., Zhang, Y., Wang, B.Y., Hakeem, A., Liu, N.N., Ou, X.W., Xu, S.F., Chen, Z.F., Lou, X.D., Xia, F., 2014. Sci. Rep. 4, 1–4.
Ke, Y.G., Sharma, J., Liu, M.H., Jahn, K., Liu, Y., Yan, H., 2009. Nano Lett. 9, 2445–2447.
Kim, K.R., Lee, Y.D., Lee, T., Kim, B.S., Kim, S., Ahn, D.R., 2013a. Biomaterials 34, 5226–5235.
Kim, K.R., Kim, D.R., Lee, T., Yhee, J.Y., Kim, B.S., Kwon, I.C., Ahn, D.R., 2013b. Chem. Commun. 49, 2010–2012.
Li, J., Pei, H., Zhu, B., Liang, L., Wei, M., He, Y., Chen, N., Li, D., Huang, Q., Fan, C.H., 2011. Acs Nano 5, 8783–8789.
Li, W., Jiang, W., Ding, Y.S., Wang, L., 2015a. Biosens. Bioelectron. 71, 401–406.
Li, Y., Wen, Y.L., Wang, L.L., Liang, W., Xu, L., Ren, S.Z., Zou, Z.Y., Zuo, X.L., Fan, C.H., Huang, Q., Liu, G., Jia, N.Q., 2015b. Biosens. Bioelectron. 67, 364–369.
Li, Z.H., Zhao, B., Wang, D.F., Wen, Y.L., Liu, G., Dong, H.Q., Song, S.P., Fan, C.H., 2014. ACS Appl. Mater. Interface 6, 17944–17953.
Liu, X., Jiang, H., Lei, J.P., Ju, H.X., 2007. Anal. Chem. 79, 8055–8060.
Liu, Z.Y., Qi, W.J., Xu, G.B., 2015. Chem. Soc. Rev. 44, 3117–3142.
Lu, N., Pei, H., Ge, Z.L., Simmons, C.R., Yan, H., Fan, C.H., 2012. J. Am. Chem. Soc. 134, 13148–13151.
Miao, P., Wang, B.D., Meng, F.Y., Yin, J., Tang, Y.G., 2015. Bioconjugate Chem. 26, 602–607.
Miao, W., 2008. Chem. Rev. 108, 2506–2553.
Pei, H., Lu, N., Wen, Y.L., Song, S.P., Liu, Y., Yan, H., Fan, C.H., 2010. Adv. Mater. 22, 4754–4758.
Pei, H., Zuo, X.L., Zhu, D., Huang, Q., Fan, C.H., 2014. Acc. Chem. Res. 47, 550–559.
Punathil, T., Tollefsbol, T.O., Katiyar, S.K., 2008. Biochem. Biophys. Res. Commun. 375, 162–167.
Qian, R.C., Ding, L., Ju, H.X., 2013. J. Am. Chem. Soc. 135, 13282–13285.

Richter, M.M., 2004. Chem. Rev. 104, 3003–3036.
Shamsi, M.H., Choi, K., Ng, A.H.C., Chamberlain, M.D., Wheeler, A.R., 2016. Biosens. Bioelectron. 77, 845–852.
Shan, Y., Xu, J.J., Chen, H.Y., 2009. Chem. Commun. 8, 905–907.
Wang, Q.L., Chen, M.M., Zhang, H.Q., Wen, W., Zhang, X.H., Wang, S.F., 2016. Biosens. Bioelectron. 79, 561–567.
Wu, P., Hou, X., Xu, J.J., Chen, H.Y., 2016. Nanoscale 8 (16), 8427–8442.
Yan, W.J., Xu, L.G., Xu, C.L., Ma, W., Kuang, H., Wang, L.B., Kotov, N.A., 2012. J. Am. Chem. Soc. 134, 15114–15121.
Yu, Y.Q., Wang, J.P., Zhao, M., Hong, L.R., Chai, Y.Q., Yuan, R., Zhuo, Y., 2016. Biosens. Bioelectron. 77, 442–450.
Yuan, L., Giovanni, M., Xie, J.P., Fan, C.H., Leong, D.T., 2014. Npg Asia Mater. 6, 1–8.
Zhang, H.R., Wang, Y.Z., Wu, M.S., Feng, Q.M., Shi, H.W., Chen, H.Y., Xu, J.J., 2014a. Chem. Commun. 50, 12575–12577.
Zhang, H.R., Wu, M.S., Xu, J.J., Chen, H.Y., 2014b. Anal. Chem. 86, 3834–3840.
Zhang, H.R., Xu, J.J., Chen, H.Y., 2013. Anal. Chem. 85 (11), 5321–5325.